SAVONIA

THESIS – BACHELOR'S DEGREE
TECHNOLOGY, COMMUNICATION AND TRANSPORT

DETERMINATION OF SAND MASS FLOW RATE IN A TEST REACTOR

AUTHOR Juuso Korhonen

SAVONIA UNIVERSITY OF APPLIED SCIENCES

THESIS
Abstract

Field of Study Technology, Communication and Transport	
Degree Programme Degree Programme in Energy Engineering	
Author Juuso Korhonen	
Title of Thesis Determination of sand mass flow rate in a test reactor	
Date 27.11.2025	Pages/Appendices 40/2
Client Organisation /Partners Valmet Technologies Oy	

Plastic has become a necessity and a permanent part of modern society. Plastic production continues to increase annually, but current recycling rates cannot keep up with the growing amount. Landfills and plastic waste hotspots keep accumulating waste, causing adverse impacts on ecosystems, economies and to human health. Plastic pyrolysis technology has gained the attention of researchers as a viable solution to address the virgin material shortage and the plastic waste recycling problem. The purpose of the thesis was to determine the bed material mass flow rate in a fluidized bed test reactor that will be later used for plastic pyrolysis. The objective was to calculate the mass flow rate which can be later used to determine mass and energy balances and applied to scale up the process to a larger model.

The research method used was a combination of experimental, qualitative, and quantitative approaches. A test matrix was created to ensure that all research questions were addressed. Methods for measuring the sand mass flow rate were evaluated. A total of seven tests were conducted in a test setup built in four shipping containers, and the bed material mass flow rate was examined in both open and closed systems, using hot and cold sand.

The sand mass flow rate was successfully measured using a scale, and it was found that pressure drop rate test was too complex and inaccurate. The maximum cold sand mass flow rate of 0,38 kg/s (SEM of ± 5,97 %) was reached when sand circulation valve, L-valve, aeration was 7 l/min and maximum hot sand mass flow rate of 0,45 kg/s (SEM 9,44 %) was reached when L-valve aeration was 4 l/min. When using hot sand, mass flow rate increased by 0,07 kg/s and the L-valve aeration dropped by 3 l/min. In the cold tests, the reactor maximum capacity of 5,5 l/min was reached at a reactor bottom pressure of 9,3 kPa, and in the hot tests, the reactor maximum capacity of 1,5 l/min was reached at reactor bottom pressure of 5,5 kPa. In the future, sand mass flow rate limitations should be investigated further, and a larger research question would be finding the optimal plastic pyrolysis process parameters for different feedstocks.

Keywords
Mass flow rate, fluidization, plastic pyrolysis

PREFACE

This thesis marks the final step in my studies in Energy Engineering at Savonia University of Applied Sciences. It was carried out to continue and address questions in the plastic pyrolysis research conducted at Valmet Technologies Oy. I am grateful for the opportunity to satisfy my curiosity and to be a part of research that truly has an impact on the global plastic problem.

I want to thank all my colleagues for creating a joyful workplace and supporting me whenever needed. In particular, I want to thank my supervisors, M.Sc. Tuomas Närhi and Ph.D. Lauri Kokko. Your work ethics and kindness have truly been inspiring, even in the presence of an impatient padawan.

I also want to thank the teachers and staff at Savonia for helping me find my career path, for teaching and challenging me, and for broadening my worldview. Thanks to Savonia, I had the opportunity to go on a study exchange, and I will always cherish the teachings of Larry Gray at Yukon University. Special thanks to my Savonia supervisors, Teija Honkanen and Petri Holopainen, for guiding me through this thesis.

Finally, I want to express my gratitude to my family for supporting me, to my beautiful wife, and to my ever-joyful dog. As my dog Hans said, the best ideas come when you leash expect, especially when you’re off the leash.

Kangasala, 27.11.2025

Juuso Korhonen

SYMBOLS

Symbol	Definition	Unit
$\dot{m}_g$	Gas mass flow rate	[g/s]
v_g	Gas velocity	[m/s]
$\dot{m}$	Mass flow rate	[kg/s]
ρ_b	Particle density	[g/cm^3]
$\dot{V}$	Volumetric flow rate	[l/min]

Acronyms	Definition
ADC	Analog-to-digital converter
CFB	Circulating fluidized bed
CO	Carbon monoxide
CO_2	Carbon dioxide
CVD	Chemical vapor deposition
DCS	Distributed control system
DEM	Discrete element method
DEN-CFD	Dense phase computational fluid dynamics
FBC	Fluidized bed combustor
FCC	Fluid catalytic cracking
H_2	Hydrogen
HDPE	High-density polyethylene
HSE	Health, safety, and environment
HTL	Hydrothermal liquefaction
LDPE	Low-density polyethylene
MFR	Melt flow rate
PC	Polycarbonate
PE	Polyethylene
PET	Polyethylene terephthalate
PLA	Polylactic acid
PP	Polypropylene
PS	Polystyrene
PSD	Particle size distribution
PUR	Polyurethane
PVC	Polyvinylchloride
SD	Standard deviation
SEM	Standard error of mean
SPI	Society of Plastic Industry

CONTENTS

LIST OF FIGURES

1 INTRODUCTION

Plastic is one of the greatest discoveries, but also one of the most harmful. As a product, it is cheap and can be used in multiple ways due to its versatile properties. Plastics can be though, flexible, transparent, and chemically resistant. Although, the benefits of plastic are clear, it presents major environmental and public health challenges (Pilapitiya & Ratnayake, 2024).

Plastics can affect both the terrestrial and aquatic animals, as they can degrade into micro plastic and even smaller nano plastic that can travel through air, water, and soil. In aquatic environments, plastic can cause problems through ingestion and entanglement, leading to ulcers, reduced reproduction, and oxidative stress. Plastics can also enter to human body through ingestion, breathing, and skin contact. Microplastic causes serious human health problems, such as cardiovascular diseases, chronic kidney diseases and birth defects (Pilapitiya & Ratnayake, 2024).

Plastic production and waste generation continue to increase annually. Therefore, more viable resources and recycling methods are needed. In recent years, plastic pyrolysis has gained attention as a potential solution to the plastic waste problem and the search of valuable resources (Dai, et al., 2022). The plastic pyrolysis process converts plastic waste into oil, gas, and char, which can be reused as virgin resource for plastic production, as a transportation fuel, or as carbon black. With this method millions of tonnes plastic waste annually produced, could be transformed as valuable resources (Peng, et al., 2022).

The purpose of the thesis is to determine the bed material mass flow rate in a test fluidized bed reactor which is a part of plastic pyrolysis setup. The objective is to calculate the mass flow rate that can be later used to determine mass and energy balances, which can be applied to scale up the process to a larger model. The thesis work is carried out for Valmet and conducted at Valmet R&D centre located in Tampere.

This thesis combines experimental, qualitative, and quantitative research. It is experimental in nature, as it involves the implementation phase of a circulating fluidized bed (CFB) and the optimization of the process based on measurements gathered during testing. The research includes qualitive elements, as phenomena occurring during implementation phase are investigated. The quantitative part of the research consists of data analysis based on the data collected from the tests.

2 PLASTICS

Plastic was invented approximately in the 1860s, and it is estimated that the plastic industry officially began in 1907. Industrial development of plastic increased significantly in the 1920s, followed by production expanding rapidly during the 1940s. By the 1950s, global plastic production reached approximately two million tons. Global plastic production has continued to increase over the following decades, reaching 368 million tons by 2019. The total consumption of plastic has increased nearly 180 times between the years 1950 – 2018 (Pilapitiya & Ratnayake, 2024).

Furthermore, over the years 2018 – 2024, global plastic production has increased by approximately 10 million tons per year (APPENDIX 1). The production rates of plastics made from bio-based, chemically recycled, and carbon captured materials represent a small fraction. Although, production of bio-based plastic has increased significantly after 2019, followed by a sharp decline in 2024. Chemical recycling has shown a steady increase, with a noticeable acceleration in 2022. Plastic production from carbon capture materials first appeared in the data in 2021 and has not increased since (Plastics Europe, 2025). Plastic made from carbon captured material means that, for example, captured carbon dioxide (CO_2) can be combined with hydrogen (H_2) to produce methanol, which can be further synthesized into olefins. The olefins produced include ethylene and propylene, which are used in plastic manufacturing (Timsina, et al., 2022), (Chen, et al., 2022) and (Mallick, et al., 2025).

Global plastic production figures vary slightly depending on the source and data available. Therefore, figures should be considered as estimates rather than facts. For instance, (Pilapitiya & Ratnayake, 2024), reported that global plastic production reached 368 million tons by 2019. However, as shown in APPENDIX 1, plastic production exceeded 370 million tons in the same year (Plastics Europe, 2025).

2.1 Plastic types and properties

The most highly produced plastics include polyethylene (PE), polypropylene (PP), polyvinylchloride (PVC), polyethylene terephthalate (PET), polyurethane (PUR), and polystyrene (PS). Table 1 presents these plastics by type according to the Society of Plastic Industry (SPI), along with their chemical structure, production percentage, and typical applications (Plastics Europe, 2025).

Table 1. Main plastic types according to the Society of Plastic Industry (SPI), chemical structure, global production share, and applications. Inspired by sources (Dai, et al., 2022), (Plastics Europe, 2025) and (Miao, et al., 2021).

Plastics	SPI	Chemical structure	Global production [%]	Applications
PET	1	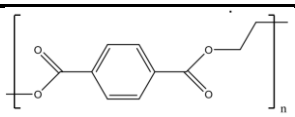	6,2	Disposable bottles, transparent food containers
HPDE	2	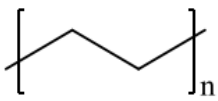	12,1	Durable containers

(continues)

Table 1 (continues).

PVC	3	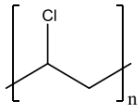	12,8	Hoses, pipes, table covers, helmets, conveyor belts, cables
LDPE	4	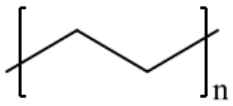	13,9	Shopping bags, bread bags, packaging film, computer components
PP	5	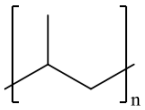	19,0	Reusable food containers, interior cushioning of luggage and seats, car parts
PS	6	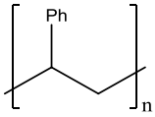	5,1	Meat trays, CD cases, Styrofoam
Other: for e.g. polycarbonate (PC)	7	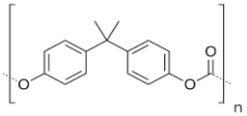	30,9	Multilayer barrier films, toothbrushes, CDs and DVDs

Note: Other plastics include production of PUR, thermosets, thermoplastics, mechanically recycled, bio-based & bio-attributed, chemically recycled and carbon captured plastics

PE, which includes high-density polyethylene (HDPE) and low-density polyethylene (LDPE), holds the largest share of production at 26 %. PUR is included in category seven which is other plastic types and therefore not shown separately in (Table 1).

2.2 Recycling methods and plastic degradation

Plastic waste recycling can be categorized into four main routes: primary, secondary, tertiary and quaternary. In primary recycling, plastic is reintroduced into the production of similar plastics. Secondary recycling, or mechanical recycling, involves the physical treatment of plastic. Tertiary recycling is a form of chemical recycling. Quaternary recycling refers to energy recovery, where the energy contained in plastic is recovered through combustion, which produces steam, electricity, or heat (Al-Salem, et al., 2010). Various processing techniques used in the four main recycling methods and the routes of plastics are illustrated in (Figure 1)

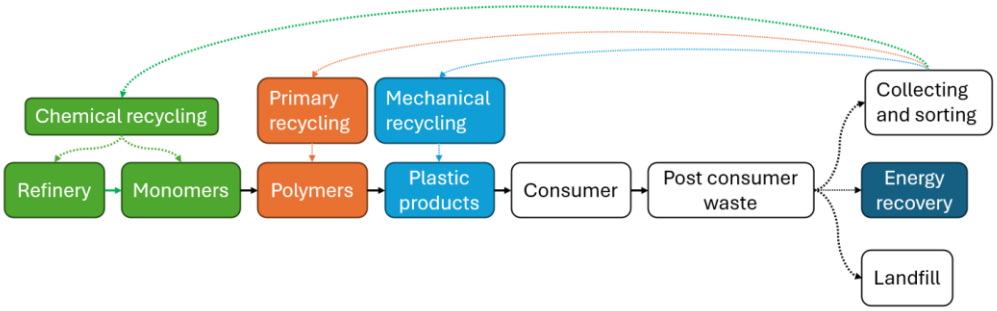

Figure 1. Four main recycling routes and their inputs to plastic production chain, inspired by (Dogu, et al., 2021)

After consumer use, plastic becomes waste and follows one of the three possible routes: recycling, incineration, or landfill disposal. Energy recovery and landfill represent end-of-life destinations of plastics (Dogu, et al., 2021). To avoid end-of-life destination and to reduce plastic production altogether, the 3R-principle can be implemented. The 3Rs stand for reduce, reuse, and recycle, where reduce is seen the most preferred option, while reuse and recycle are less favourable alternatives. Reduce refers to minimizing the production and use of plastic. Reuse involves designing products for repeated use, such as washable or returnable containers. Finally, recycle means processing of plastic waste as a raw material for new products (Pilapitiya & Ratnayake, 2024). From the total plastic waste generated annually, only about 7 % is recycled, while the remaining majority ends up to end-of-life destinations (Kalali, et al., 2023).

After production, plastic begins to degrade due to of environmental weathering shown in (Figure 2). Slow degradation process starts immediately after the plastic product is manufactured (Zhang, et al., 2021).

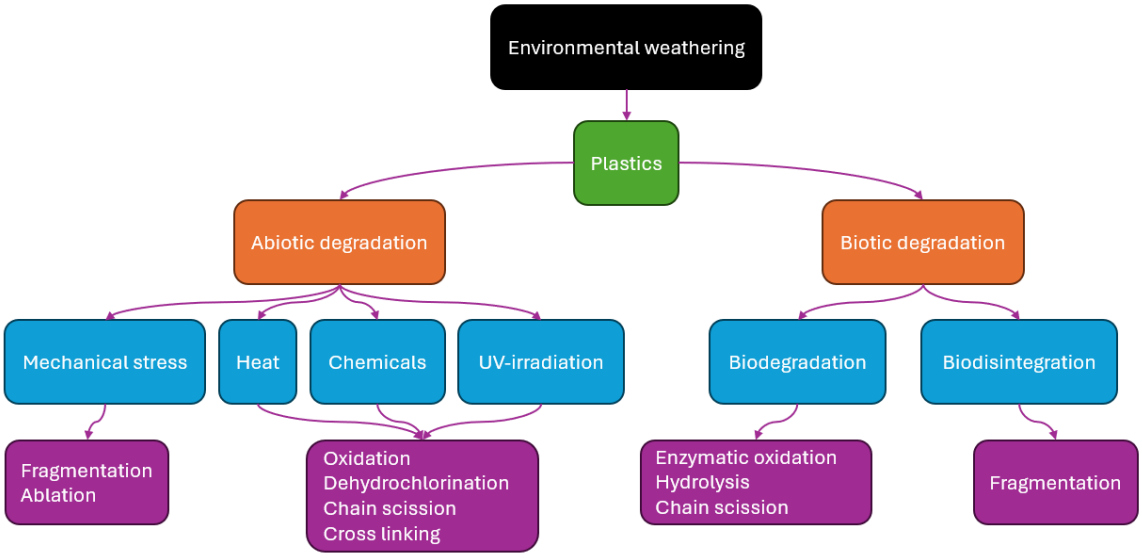

Figure 2. Plastic degradation due to environmental weathering, inspired by (Zhang, et al., 2021)

Plastic degradation is a slow process that breaks down plastics and leads to changes in polymer properties. The environmental weathering of plastic can occur due to abiotic degradation, biotic degradation, or a combination of both. Abiotic degradation is a change in the physical or chemical properties, occurring due to factors such as light, temperature, air, water, and mechanical forces. Biotic degradation is the breakdown of plastic by organism. It occurs when organisms physically degrade plastics by biting, chewing, or consuming them. Microorganisms, such as bacteria, fungi and insects, are among the most common reason to biotic degradation (Zhang, et al., 2021).

Furthermore, mechanical stress result in fragmentation and ablation meaning loss of material from the surface. Fragmentation can also occur during biodisintegration. Heat, chemicals and UV-irradiation can cause oxidation, dehydrochlorination, chain scission and cross linking of plastic polymers. Biodegradation can lead to enzymatic oxidation, hydrolysis and chain scission. Due to

these factors, plastic recycling is difficult because the properties of plastic have weakened during the use. (Zhang, et al., 2021).

2.2.1 Mechanical recycling

Mechanical recycling is a process in which plastic waste is reused in the production of new plastic through mechanical methods. This involves the use of recycled materials, fillers, additives and virgin polymers (Al-Salem, et al., 2010). According to (Ragaert, et al., 2017), mechanical recycling of waste plastics begins after collection. The process consists of five steps, as shown in (Figure 3). These steps can be repeated or excluded, depending on the condition of plastic and the desired outcome.

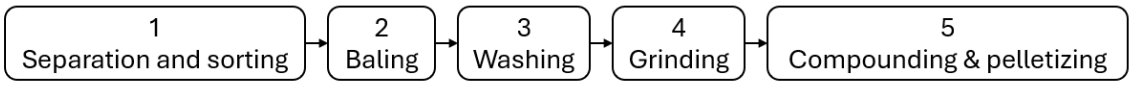

Figure 3. Steps in mechanical recycling process, adapted from (Ragaert, et al., 2017)

The mechanical recycling starts with separation and sorting. This step is based on characteristics such as shape, density, size, colour, or chemical composition. If the plastic is not processed on the site, it is baled for transportational purposes. The purpose of the washing stage is to remove contaminants, often organic. Grinding is then performed to reduce size of the plastics into flakes. Finally, compounding and pelletizing is an optional step that reprocesses the flakes into granules, making them easier for converters to use (Ragaert, et al., 2017).

The plastic degradation mechanisms can be divided into three categories: thermal degradation, mechanical degradation, and thermal oxidative degradation. Typical properties that change due to any type of degradation include viscosity, melt flow rate (MFR), molecular weight, thermal properties, and mechanical properties. In a study, PE, PP and their blends were subjected to five consecutive twin-screw extrusion cycles to simulate thermo-mechanical recycling. Results showed that PP crystal structure was affected and generated disorder. However, tensile properties did not diminish but all the other properties had a decreasing trend (Saikrishnan, et al., 2020).

The disadvantages of mechanical recycling are that it is only suitable for single-polymer plastics, and the more complex and contaminated the plastic waste is, the harder it becomes to recycle. One of the obstacles of mechanical recycling is the plastic degradation and heterogeneity (Al-Salem, et al., 2010).

2.2.2 Chemical recycling

As stated earlier, the quality of products made from mechanically recycled plastic remains a core problem that must be addressed with alternative viable solutions (Al-Salem, et al., 2010). One of the potential solutions is chemical recycling shown in (Figure 4). During chemical recycling process plastic waste is converted into small molecules that can be either liquid, gas or solids. Products can be reused as fuels, agents or building blocks for new plastic products. Plastics made from the

chemically recycled materials are same quality as virgin plastics. This means that plastic produced can be used in industries that require high quality products such as food packaging. (Liu, et al., 2024).

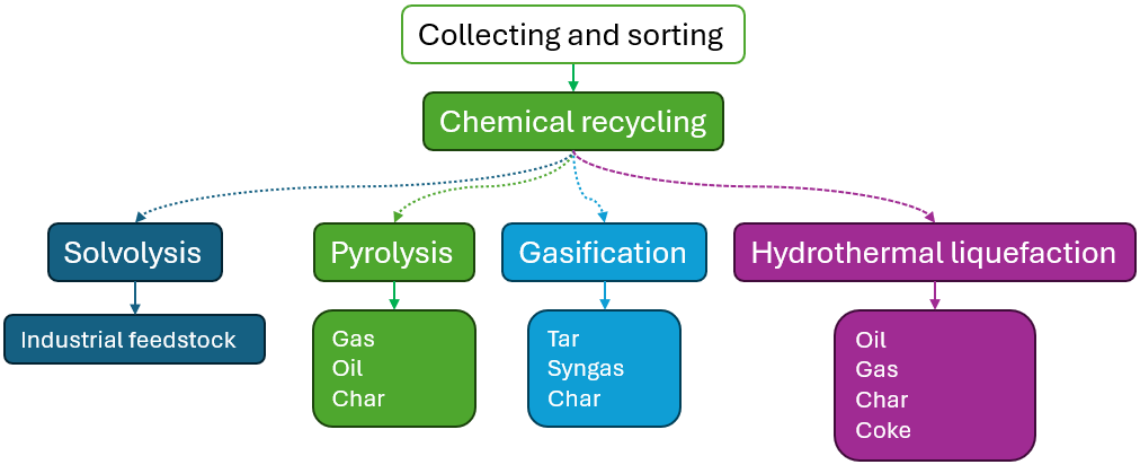

Figure 4. Chemical recycling methods, adapted from (Liu, et al., 2024)

Chemical recycling can divide into four methods. Solvolysis, pyrolysis, gasification, and to hydrothermal liquefaction (HTL) shown in (Figure 4). These methods can be roughly categorized by temperature used and the nature of bond cleavage. Solvolysis is an effective method for plastic such as PET, polylactic acid (PLA), PC, and PS. Plastics like LDPE, HDPE, and PP are better suited for pyrolysis, although the process can manage PET and PVC, these are not optimal. HTL and gasification are suitable for wider range of plastics, although chloride compounds of PVC cause corrosion to the system (Liu, et al., 2024).

Solvolysis is also known as depolymerization, referring to the methodical breakdown of a polymer into monomeric units. The process can be conducted with or without a catalyst and the product depends on the solvent used. Solvolysis is usually conducted in a temperature between 65 – 240 ºC (Liu, et al., 2024).

In the gasification process, high temperatures of 700 – 1000 ºC are used to maximize the syngas yield from plastic waste. Gasification products are syngas mainly consists of carbon monoxide (CO) and H_2, tar and char. The main differences of pyrolysis and gasification are the higher temperature of gasification and oxygen used in the process (Liu, et al., 2024).

HTL refers to process where supercritical water works as a solvent and catalyst. During this process temperature ranges between 350 – 500 ºC. Advantages of HTL are preventions of side reactions and removal of impurities such as halogen, and nitrogen, and oxygen compounds. Disadvantages of HTL is that process is highly corrosive and therefore chemically resistant alloys are needed. The main products of HTL are oil, gas, char and coke. (Liu, et al., 2024).

Plastic pyrolysis is a process in which long-chain polymer molecules are thermally degraded into smaller chains by heat and pressure. The process happens in absence of oxygen, relatively fast, and requires intense heat of approximately 500 ºC. However, in plastic pyrolysis studies, the

temperature varies between 350 – 740 ºC. The three main products of the pyrolysis process are oil, gas and char, which are in high demand in industries, especially in production and refineries (Dayana Anuar Sharuddin, et al., 2016).

Compared to other chemical recycling methods, plastic pyrolysis has a high technological readiness for maximizing the oil yield (Solis & Silveira, 2020). This is because it can process mixed plastic waste and make use of the existing infrastructure and expertise. In addition, the pyrolysis process produces valuable chemicals from pyrolysis oil and generates gases that can be converted into heat and electricity to power its own operations (Liu, et al., 2024).

3 FLUIDIZED REACTORS

Fluidized reactors have a long history, beginning with Winkler's coal gasifier in the 1920s (Kunii & Levenspiel, 1991). Following the first application, fluidization has evolved through three cycles that can be seen in (Figure 5). Each of which can be further divided into three development stages: the phenomenological stage, the structural stage, and the essential stage. These stages follow the progress of a science introduced by Taketani in 1942 (Horio, 2010).

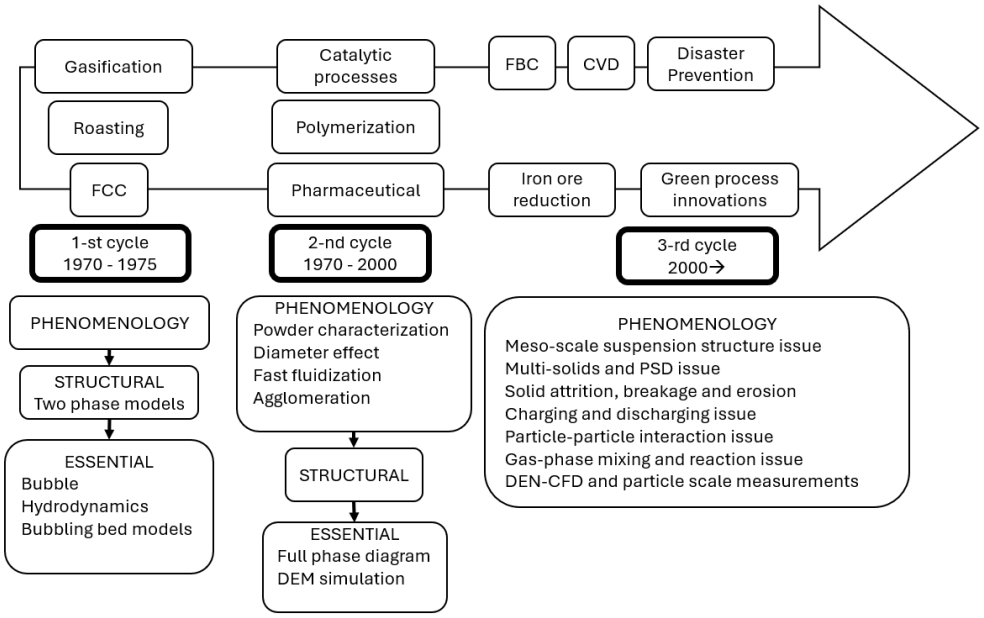

Figure 5. Development of fluidization technology and science, inspired by (Horio, 2010)

It is estimated that the first cycle began in the early 1940s.The second step took place in the 1950s when two-phase theory was introduced. Two-phase theory conceptualized that fluidized bed consists of bubble and emulsion phases. The third stage occurred in the 1960s when bubble hydrodynamics was introduced. The second cycle was in the years between 1975 – 2000. During this period, the well-known CFB was introduced. The third cycle started in the 2000 and it is still on going in the phenomenology stage (Horio, 2010).

3.1 CFB reactor in plastic pyrolysis

Plastic waste presents significant challenges during pyrolysis compared to other solid wastes, due to its low thermal conductivity, sticky nature, low softening and melting temperature. Therefore, efficient heat transfer and advanced reactor design are essential. Common reactor types that address the heat transfer issues and are suitable for industrial applications are screw kiln reactors and fluidized bed reactors. CFB reactor is relatively easy and more affordable to scale up compared screw kiln reactor. CFB reactor also possess good characteristics to address common problems during plastic pyrolysis. They are known for their high heat and mass transfer rates, effective mixing, and good control of operational parameters (Dai, et al., 2022).

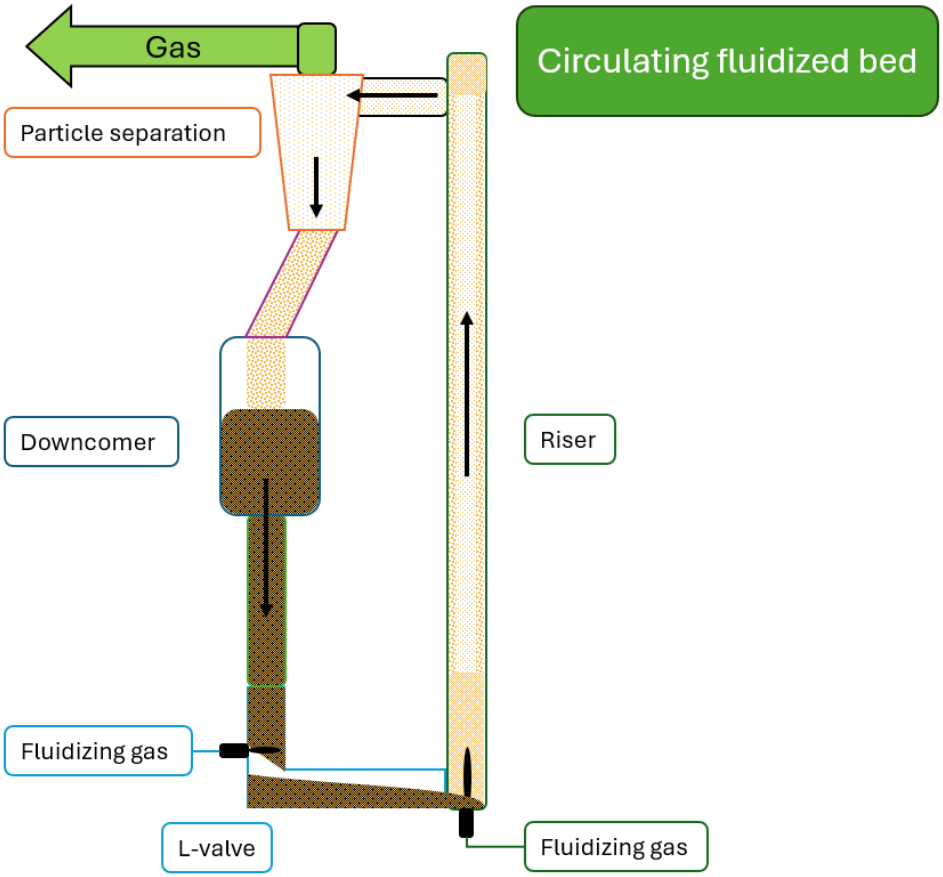

Figure 6. Typical CFB configuration (Korhonen, 2025a)

A typical CFB consists of four main components: a riser, a particle separator, a downcomer, and a L-valve (Figure 6). In this configuration L-valve supplies solids to riser. The fluidization gas of the riser is provided from the bottom. A point is reached where all the solids are suspended by the upward flowing gas. At this point, the frictional force between the solids and fluid counterbalances the weight of the solids and fixed bed transitions into minimum fluidization. If the fluidization is increased further, bed goes through a series of phases. When the terminal velocity of solids is exceeded, a phase called turbulent fluidization, or lean phase fluidization, is reached, and the bed starts to disappear from the top of the riser (Kunii & Levenspiel, 1991).

The bed needs to be recirculated, and to achieve this, the gas and solids must be separated. In this configuration a cyclone is used, in which solids are separated by a radical centrifugal force. Solids are driven to the cyclone wall, where they slide into downcomer. Cyclones are widely used since they have no moving parts, they are relatively cheap to construct and to maintain. (Muschelknautz & Greif, 1997)

A downcomer or a standpipe is a vertical return pipe. Solids can travel in the standpipe by gravity in a dilute or in a dense phase from cyclone to the L-valve. The basic principle of a standpipe is to transfer solids from a lower pressure, near the outlet of circulating bed to a higher pressure at the bottom of the bed. L-valve is a common non-mechanical valve, and the name comes from the shape. Solids flow through a valve because of drag forces on the particles produced by the aeration

gas. The amount of solid flow is controlled by the aeration gas added to the L-valve (Knowlton, 1997).

One of the limitations to the industrial operation of CFB is the choking phenomenon. This commonly happens in the riser when the fluidization flow rate is too low to keep solids in a fluidized state. During choking, the bed becomes dense, and solids settle, causing pressure drop, instability and blocked flow. Choking can be avoided by increasing the riser height relative to diameter of the reactor. However, if ratio is disproportionate radical cluster bubbles may occur causing slugging (Xiao, et al., 2024).

4 STATISTICAL ANALYSIS

Data analysis is a part of quantitative research. Common approach is statistical analysis, where understanding the variability and reliability of data is necessary for drawing accurate conclusions. Two widely used statistical analysis measurement methods are standard deviation (SD) and standard error of mean (SEM).

Standard deviation (SD) is an index how closely individual data points cluster around the mean. Standard error of mean (SEM) measures how mean indicates the range of calculated mean. In a way it measures the adequacy of the sample. By taking more measurements, SEM decreases. In other words, the certainty of mean's accuracy improves as the sample size increases. To calculate SEM, the SD must be determined (Hassani & Ghodsi, 2010).

SD can be calculated as:

$$SD = \sqrt{\frac{\sum_{i=1}^{N}(X_i - \bar{x})}{N-1}}, in\ which \quad (1)$$

- X_i is the value of data point
- $\bar{x}$ is the population mean
- N is the population size

SEM can be calculated as:

$$SEM = \frac{SD}{\sqrt{N}} \quad (2)$$

Both SD and SEM are important tools in statistical analysis. These methods form a basis for drawing reliable conclusion from a raw data. Without statistical tools, wrong conclusions could be drawn, as the mean value alone does not provide information about the SD or from the SEM. Therefore, use of statistical methods is essential.

5 TEST GOALS AND TEST SETUP

The purpose of the thesis was to determine the bed material mass flow rate in a test fluidized bed reactor that will be used for plastic pyrolysis after the thesis work. The objective was to calculate the mass flow rate which can be later used to determine mass and energy balances and applied to scale up the process to a larger model.

The research questions were: (1) What is the maximum capacity of the L-valve and the test setup, and (2) how do these change when hot or cold bed material is used?

The setup was built into four intermodal containers that were constructed in three vertically stacked intermodal containers, while the fourth one served as a control room. The test setup is shown in (Figure 7).

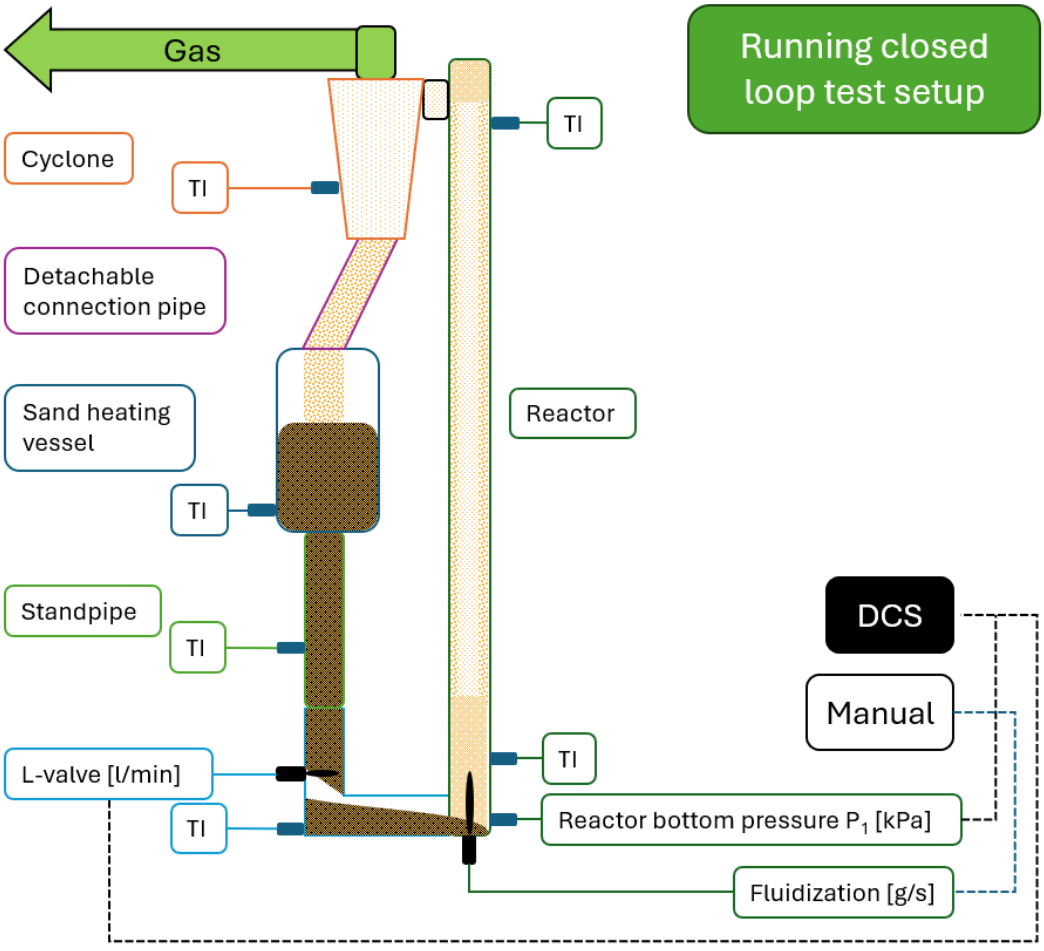

Figure 7. Running closed loop test setup (Korhonen, 2025b)

The key components in the test setup were the fluidized bed reactor, cyclone, sand heating vessel, standpipe and L-valve. The process was operated from the control room or manually from the field, depending on the test.

5.1 Test matrix

Before starting the tests, a test matrix was created (Table 2). Purpose of the test matrix was to function as guideline according to which all research questions would be systematically answered. However, both the test matrix and the test setup had to be modified during testing to achieve necessary results.

Table 2. Test matrix

Test	Temp	Method	Reactor fluidization gas $\dot{m}_g$ [g/s]	Reactor fluidization velocity v_g [m/s]	L-valve aeration $\dot{V}$ [l/min]	Tests
1	Cold	Manual stop	15	4,8	4	5 repetitions
2	Cold	Automatic stop	15	4,8	4	5 repetitions
3	Cold	Open	15	4,8	4 – 5 – 6 – 7 – 8,3 – 9,7	5 each
4	Hot	Open	5,5	4,8	2	5 repetitions
5	Hot	Open	12	10,5	1 – 9 in steps of 1	1 each
6	Cold	Closed	15	4,8	0 – 9,5 in steps of 0,5	1 each
7	Hot	Closed	5,5	4,8	0 – 9,5 in steps of 0,5	1 each
			Deviation from target ± 1,33 %	Deviation from target ± 9,66 %		

Note: “Temp” refers to the temperature used in a test, in general terms. “Method” describes how the test setup is operated.

Air was used as a fluidization gas in the tests. Reactor fluidization velocity was calculated using (Equations 7 – 13). During the cold tests, the sand temperature was determined by ambient temperature and therefore it changed throughout the day. When the reactor internal temperature of 20 ºC varied by ± 10 ºC at a pressure of 5 kPa, air viscosity changed by approximately ± 3 % and density by about ± 3,5 %

5.2 Safety

Valmet R&D centre has four different level risk assessment methods to ensure safety of the work. Before conducting any work, risks were evaluated, and the level was chosen accordingly. For smaller risks, the risk handbook was filled.

The safety of the work was evaluated through a risk assessment level 2. Risk assessment was conducted before starting the hot fluidization tests. It was supervised by health, safety and environment (HSE) expert. The method involved a discussion with participating parties about the possible risks during operation and a walkaround on the project site.

Based on the discussion and walkaround, risks were listed and the current state of the risk evaluated. If a risk was not in order, a solution had to presented and the solution completion was monitored. The most concerning risks during the tests were the hot sand and floating sand dust particles. In addition, commonsense and consideration before acting was highlighted.

During research, standardized clothing was used according to Valmet guidelines (Valmet, 2025). Such as helmets (EN 397), (SFS, 2025), shoes (EN ISO 20345), (SFS, 2022), eye and face protection (EN ISO 16321), (SFS, 2022) and hearing protection (EN 352-1), (SFS, 2020), gloves fitting to work, and fire protected clothing (EN ISO 11612), (SFS, 2015).

The sand was warmed in a sand heating vessel using ceramic band heaters. Hot sand could cause burn wounds and was at the highest risk when emptying the scale and filling up the system again. The scale vessel was made of metal, and under the scale was a protective metal sheet to prevent the hot sand spilling from the middle container to the bottom container. When moving the sand to the uppermost container, it was important that only one person was allowed on the staircase at a time, and buckets were carried individually. Also, heat-protective gloves were used, and firefighting foam and flame-retardant fabric was available.

The sand used in the test was natural sand and therefore contained quartz dust, which can cause severe respiratory diseases and eye irritation (Eskanlou & Arnold, 2025). The risks were reduced by using powered air-purifying respirator. In case of emergency, eye-washing fluid and a safety shower was also available.

5.3 Preparations

The bulk density of the sand and the reactor gas fluidization velocity had to be determined. The sand used in the test was Fescon's natural sand, size distribution 0,0 – 0,25 mm (Fescon Technology, 2025). Fescon follows the sample collection standard SFS-EN 932-1 (SFS, 2012) and testing instruction standard SFS-EN 933-1 (SFS, 2012).

Bulk density of sand was determined using a scale and measuring cup shown in (Figure 8). Bulk density can be used for calculating mass when the volume is known. Once the mass is determined, the mass flow rate can be calculated by dividing the mass by the time needed to fill the measuring vessel. This is common practice during a bigger cold fluidization test.

Figure 8. Measuring cup (Korhonen, 2025c, CC-BY)

Calculating the mass m when the volume V is known:

$$m = \rho_b V \tag{3}$$

When the mass m and time t is known the mass flow rate $\dot{m}$ can be solved:

$$\dot{m} = \frac{m}{t}, in\ which \tag{4}$$

- m is the mass of the sand in [g]
- t is the time in [s]

The next step was to load the process from the connection pipe above the sand heating vessel. The measurement was done using a scale, subtracting the bucket's weight from the total sand mass shown in (Figure 9). Total sand mass during the test was 52 500 g. After loading the sand heating vessel, the process loop was closed.

Figure 9. Sand bucket on a scale (Korhonen, 2025d, CC-BY)

The bulk density ρ_b was determined as:

$$\rho_b = \frac{m}{V}, in\ which \tag{5}$$

- m is the mass of the sand in [g]
- V is the volume that sand takes in [cm^3]

$$\Longrightarrow \rho_b = \frac{4709\ g}{3000\ cm^3} = 1{,}57\ g/cm^3 \tag{6}$$

To solve reactor fluidization velocity v_g, the volumetric flow rate of gas in the reactor $\dot{V}$ had to be solved using the general gas equation:

$$P\dot{V} = \dot{n}RT, in\ which \tag{7}$$

- P is the pressure in [Pa]

- R is the universal gas constat in [J/mol K]
- T is the gas temperature in [K]
- $\dot{V}$ is the volumetric flow rate of gas in [m^3/s]
- $\dot{n}$ is the molar amount of gas in [mol/s]

The molar amount of gas was solved using equation:

$$\dot{n} = \frac{\dot{m}_g}{\dot{M}}, in\ which \tag{8}$$

- $\dot{m}_g$ is the mass flow rate of reactor fluidization gas in [g/s]
- $\dot{M}$ is the molar mass of air in [g/mol]

$$\Longrightarrow \dot{n} = \frac{15\ g/s}{28{,}97\ g/mol} = 0{,}52\ mol/s \tag{9}$$

The reactor volumetric flow rate was determined as:

$$\dot{V} = \frac{\dot{n}RT}{P} \tag{10}$$

$$\Longrightarrow \dot{V} = \frac{0{,}52\frac{mol}{s} * 8{,}314\frac{J}{mol * K} * 286{,}36\ K}{\frac{1053\ Pa}{2} + 101325\ Pa} = 0{,}012\ m^3/s \tag{11}$$

Finally, the gas velocity in the reactor can be determined as:

$$v_g = \frac{\dot{V}}{A}, in\ which \tag{12}$$

- A is the reactor cross sectional area, 0,0025 m^2

$$\Longrightarrow v_g = \frac{0{,}012\frac{m^3}{s}}{0{,}0025\ m^2} = 4{,}9\ m/s \tag{13}$$

5.4 First test

The first test aimed to determine the mass flow rate of cold sand using a closed loop stop test. Test setups are shown in (Figure 10 and Figure 11). The Figure 10 shows the starting point where preparations had been completed, and the Figure 11 displays the running process. In this configuration, the valve in the connection pipe was closed. The sand circulation time from the sand heating vessel to the cyclone was measured from the DCS analysing reactor pressure difference.

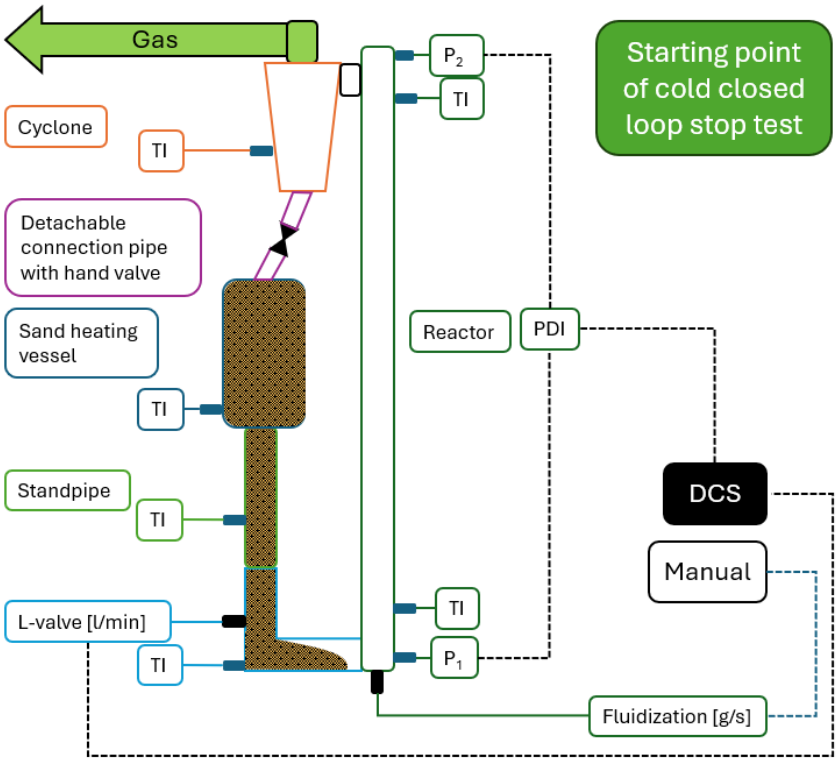

Figure 10. Starting point of cold closed loop stop test (Korhonen, 2025e)

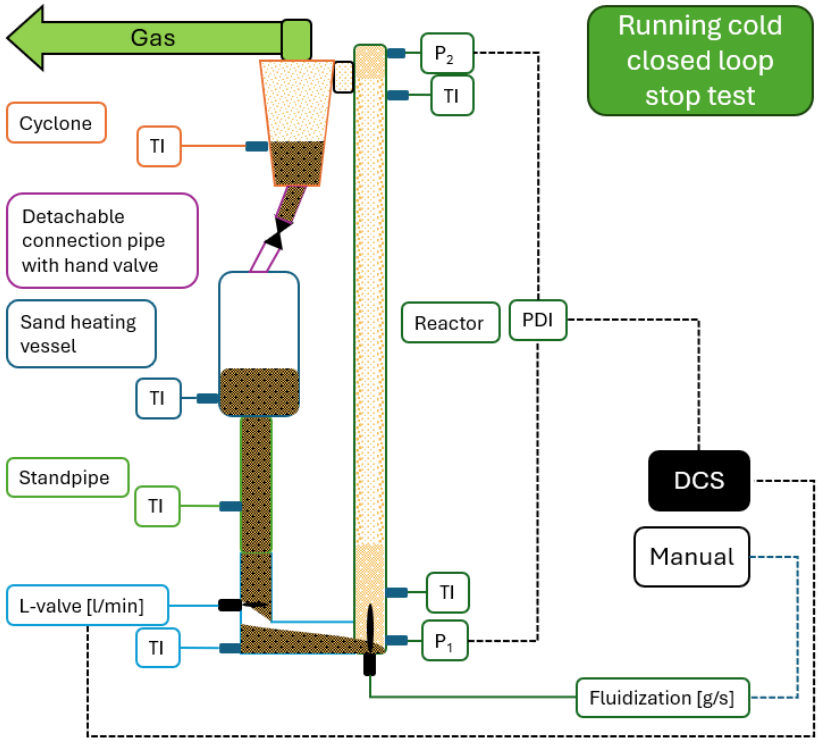

Figure 11. Running cold closed loop test (Korhonen, 2025f)

The test was started by adjusting the reactor fluidization using a rotameter. Next, the data collection was started from the DCS, and the L-valve was opened. The goal was to do five repetitions with the same parameters to get accurate results. Due to multiple problems, nine stop tests had to be done to achieve one representative result.

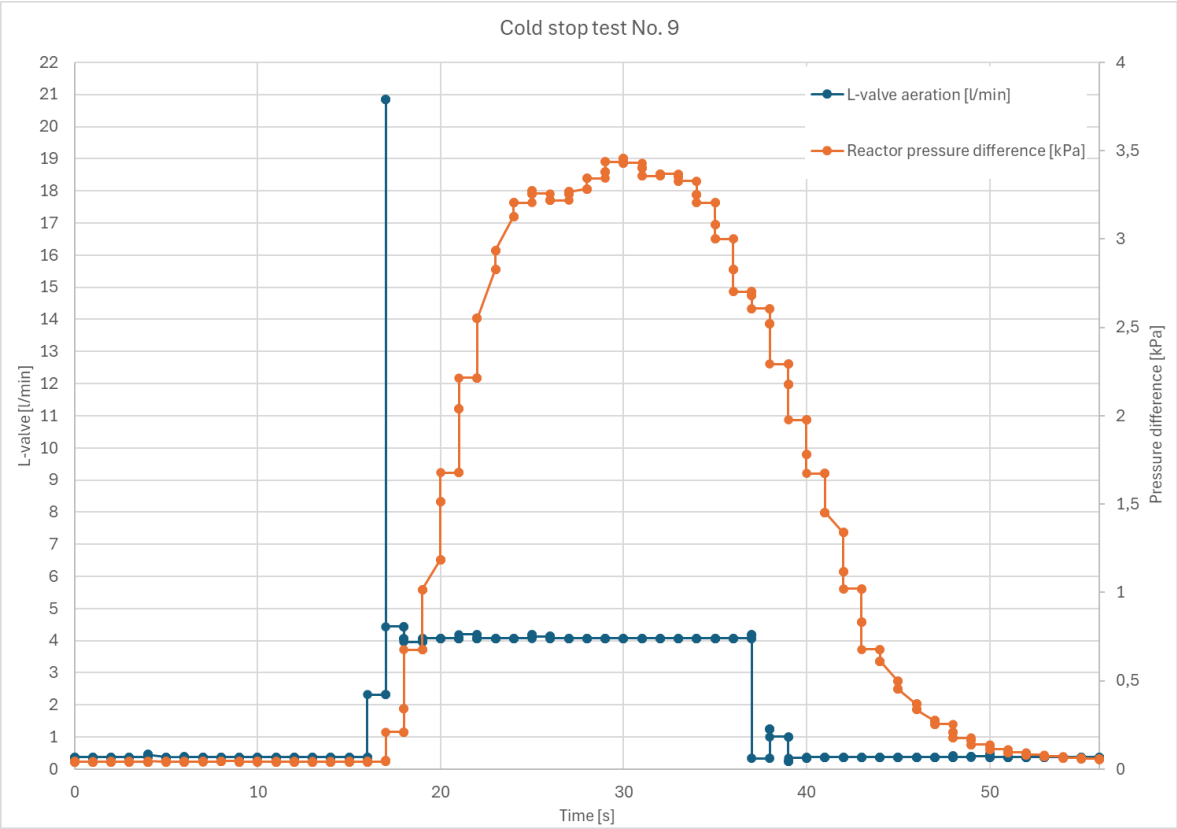

Figure 12. Cold stop test No. 9 (Korhonen, 2025g)

Figure 12 shows the analysed results from the cold stop test. At the start of the test, there was a noticeable delay in the reactor pressure difference. It was predicted that sand was packed in the standpipe and L-valve could not aerate the sand immediately. In the middle phase, the pressure difference was representative, but this lasted approximately 10 seconds. Towards the end of test, the pressure difference lingered. It was estimated that pressure difference decreased exponentially assuming that the mass flow rate out of the reactor was directly proportional with the sand mass inside the reactor.

The method used was not accurate enough to determine the mass flow rate. The reactor pressure difference gave faulty readings. This was probably due to the plugging of the pressure measurement connection line P_2. This was seen from data as negative numbers or the pressure difference was not changing as intended (APPENDIX 2). Despite not achieving the desired results, the process was running for the first time. It provided insight about the maximum sand volume in the system. An approximate sand mass flow rate was calculated. The initial calibration of L-valve was successful, and the DCS started working as intended.

5.5 Second test

The purpose of the second test was to determine the sand mass flow rate based on the pressure difference drop rate. The test was conducted using a sequence that automatically opened and closed the L-valve. To analyse the results, it was assumed that when the L-valve stopped, sand continued to flow out of the reactor momentarily at the same rate as when the L-valve was open. The theory was that pressure difference drop rate decreased exponentially and was proportional to

the rate at which the sand mass decreased in the reactor. Therefore, the mass flow rate could be determined.

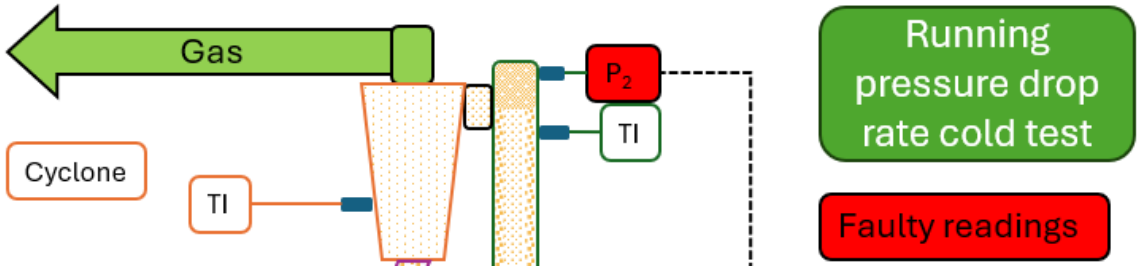

Figure 13. Faulty pressure line (Korhonen, 2025h)

Test was unsuccessful due to the reactor pressure difference was giving a faulty reading. Plugged P_2 line is highlighted with red in (Figure 13). Another reason for not continuing with this method was due to complexity and the difficulty of obtaining accurate and repeatable measurements.

After the second test, the process was emptied, and total of 36 807 g of sand was collected. The total sand input was 52 500 g, of which 6 876 g escaped further into process and was collected from the sample valve. Therefore, 8 817 g remained in the process, most likely in the L-valve, and in the horizontal connection pipes. In addition, the cyclone and the sand heating vessel had relatively flat bottoms instead of cone shaped. Because of this, more sand is going to stay in these parts.

5.6 Third test

The objective of the third test was to determine the mass flow rate of cold sand in an open loop and to examine how the change in L-valve aeration affects the mass flow rate. The test figuration is shown in (Figure 14 and Figure 15). The Figure 14, shows the starting point of the test, and the Figure 15, shows the test running. During the test, connection pipe was detached from the cyclone. An extra pipe was installed to the cyclone. The sand coming from the cyclone was directed to the scale, and the original pipe guided the sand to the heating vessel during the filling.

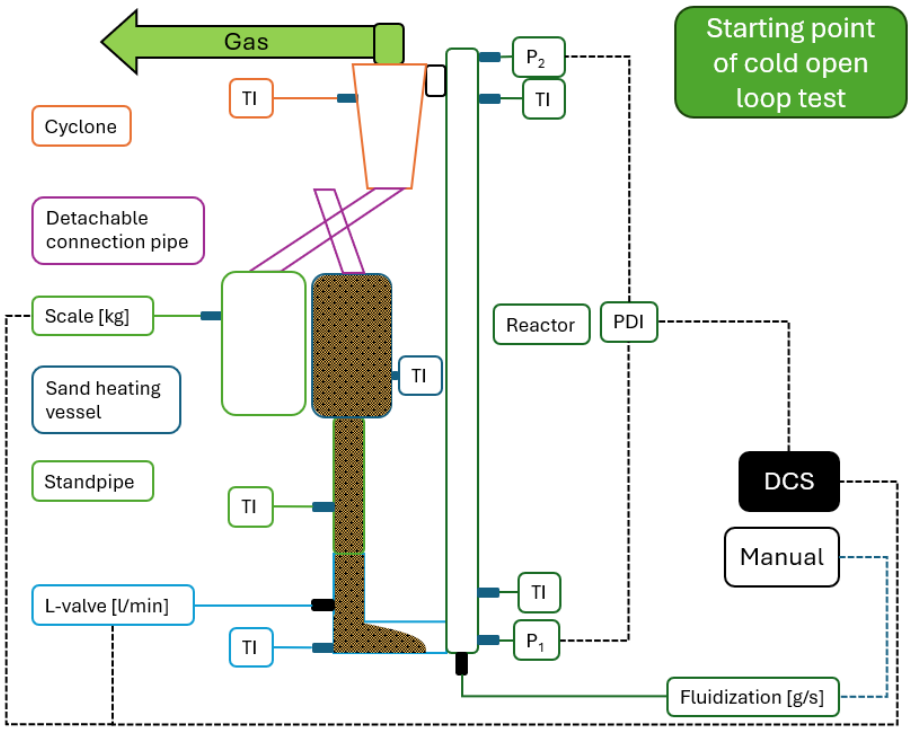

Figure 14. Starting point of cold open loop test (Korhonen, 2025i)

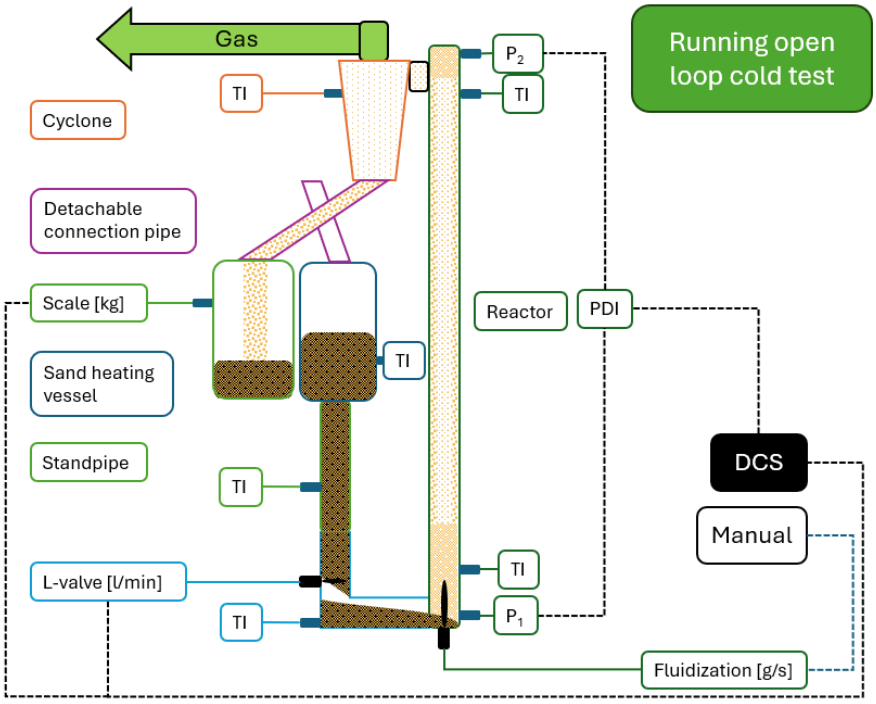

Figure 15. Running open loop cold test (Korhonen, 2025j)

Before starting the third test, the scale had to be connected to the DCS and calibrated. This was done to ensure that the scale readings are accurate. The first step of the calibration was to measure the sand and pour it into the sand heating vessel. After this, the L-valve and the reactor fluidization were turned on, and the sand started to circulate to the scale connected to DCS.

Table 3. Scale calibration data collected from DCS, inspired by (Peterson, 2023)

Sand m [g]	Signal
0	300
12083	1028
23368	1709
34116	2358
46452	3105

Note: Signal standard value range 0 – 27648

The next step was to collect the data from the DCS, as shown in Table 3, and to examine the correlation coefficient between the sand mass and the signal. It is notable, that the signal doesn't have a unit. This is because the signal output from the scale is analog signal in mA. Scale signal goes to analog-to-digital converter (ADC). Signal output from the ADC goes to the programmable logic controller (PLC). Signal value is then converted to a standard value range of 0 – 27648 that can be displayed (Peterson, 2023). The mass values are presented on the left, and the corresponding signal values are shown on the right (Table 3). Based on the data, figure could be created and the accuracy of scale evaluated (Figure 16).

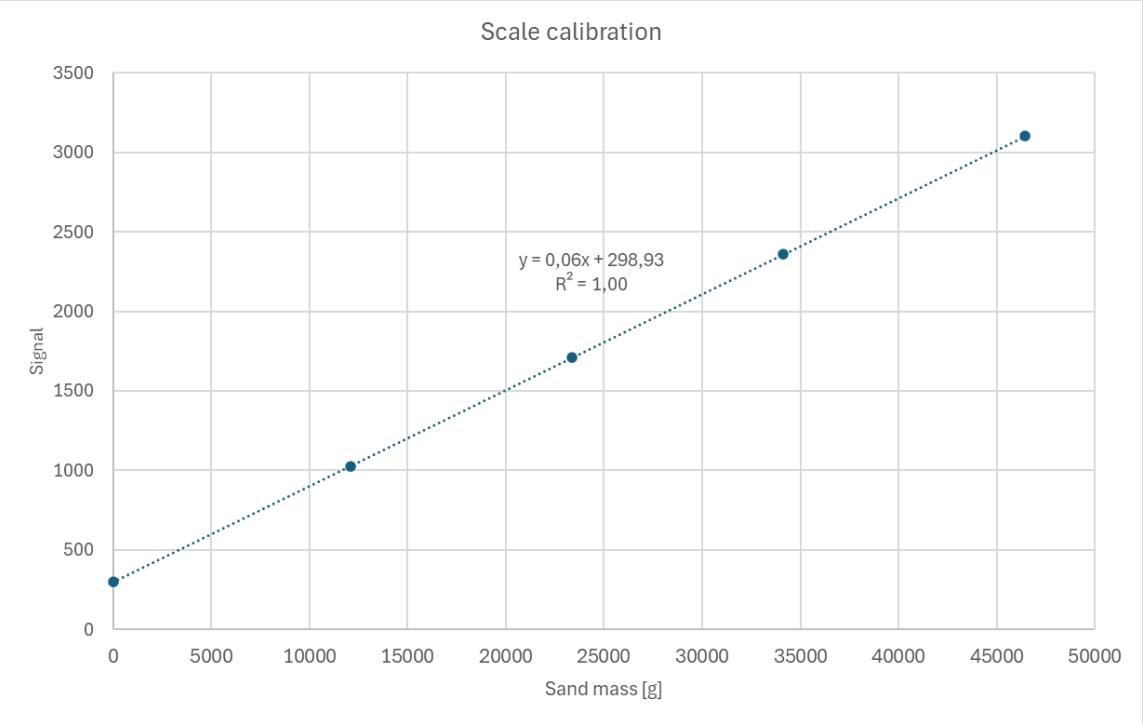

Figure 16. Scale calibration data analysis (Korhonen, 2025k)

By examining Figure 16, it was determined that scale calibration was successful. This was since the correlation coefficient (R^2) between the signal, and the sand mass was 1,00, which shows a perfect correlation, therefore scale functions accurately.

The next step was to fill the sand heating vessel and to start the open loop cold test according to the test matrix shown in (Table 2). In the third test, the process was open loop and cold sand was used. The test setup was built outdoors, and during the cold test, no added heat was applied to the setup. Therefore, the temperature of cold sand was close to the ambient temperature. The L-valve aeration was controlled from the DCS, starting at 9,7 l/min. The test reactor fluidization was manually adjusted using the rotameter to 15 g/s, which corresponds with 4,8 m/s.

After scale was calibrated, the system was loaded with sand, and the L-valve aeration and the reactor fluidization was set according to the test matrix. Series of six tests were performed with five repetitions from each L-valve aeration volume rates shown in (Figure 17).

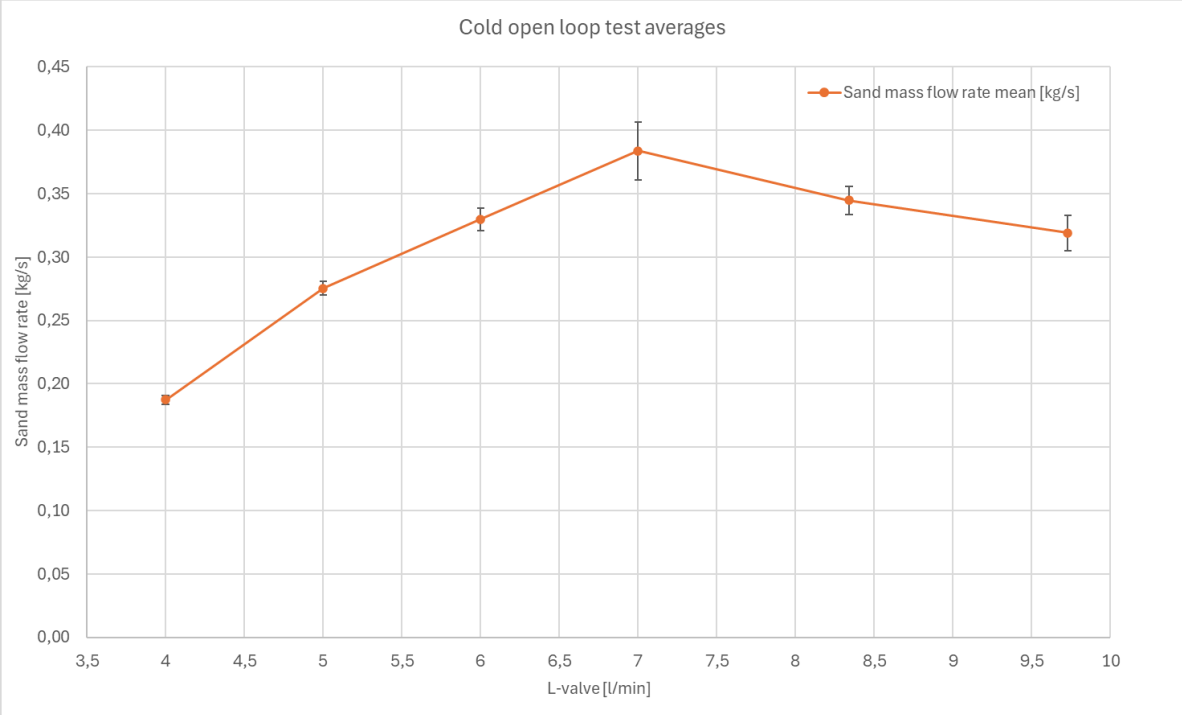

Figure 17. Cold open loop test averages (Korhonen, 2025l)

Test results were evaluated by calculating the standard deviation (SD) and the standard error of mean (SEM) as presented in (Equation 1 – 2). The SEM values are displayed in Figure 17 as error bars. From the total of 30 cold open loop tests that were conducted, it is noticeable that maximum sand mass flow rate was achieved when the L-valves aeration was 7 l/min. At this point SEM was also at its highest. It is also notable that the first 10 kg and the last 10 kg of sand, along with the corresponding data, were removed to ensure the data was as representative as possible.

Test was successful, since the number of unknown values was low, data collection was relatively fast, and it was possible to obtain reliable and accurate test results. It is worth mentioning that the setup was simple to understand and use.

5.7 Fourth and fifth test

For the fourth and fifth test, the sand was changed to hot varying in between 485 – 550 ºC, while the test setup remained the same. The goal of the fourth test was to make a repetition series with assumed standard L-valve operating value of 2 l/min. Five repetitions were made, and data is presented in (Figure 18). This was done to obtain more accurate results and to gain understanding how the SEM diminishes when the amount of the tests is increased. SEM is visualized as horizontal error bars. The purpose of the fifth test was to gain broader picture from the sand mass flow rate by changing the L-valve aeration.

In the fourth test, the reactor fluidization mass flow rate was set to a relatively low value of 5,5 g/s, which corresponds with 4,8 m/s. The pyrolytic vapours produced during the plastic pyrolysis process adds up to the overall gas flow and therefore increase the reactor fluidization velocity, for which reason the reactor fluidization was set to low value (Sing, et al., 2016).

In the fifth test, the fluidization mass flow rate was 12 g/s, which corresponds with 10,5 m/s. The L-valve aeration was increased in 1 l/min increments within the range of 1 – 9 l/min. The results from the fourth test (blue) were compared to the fifth test (orange) in (Figure 18).

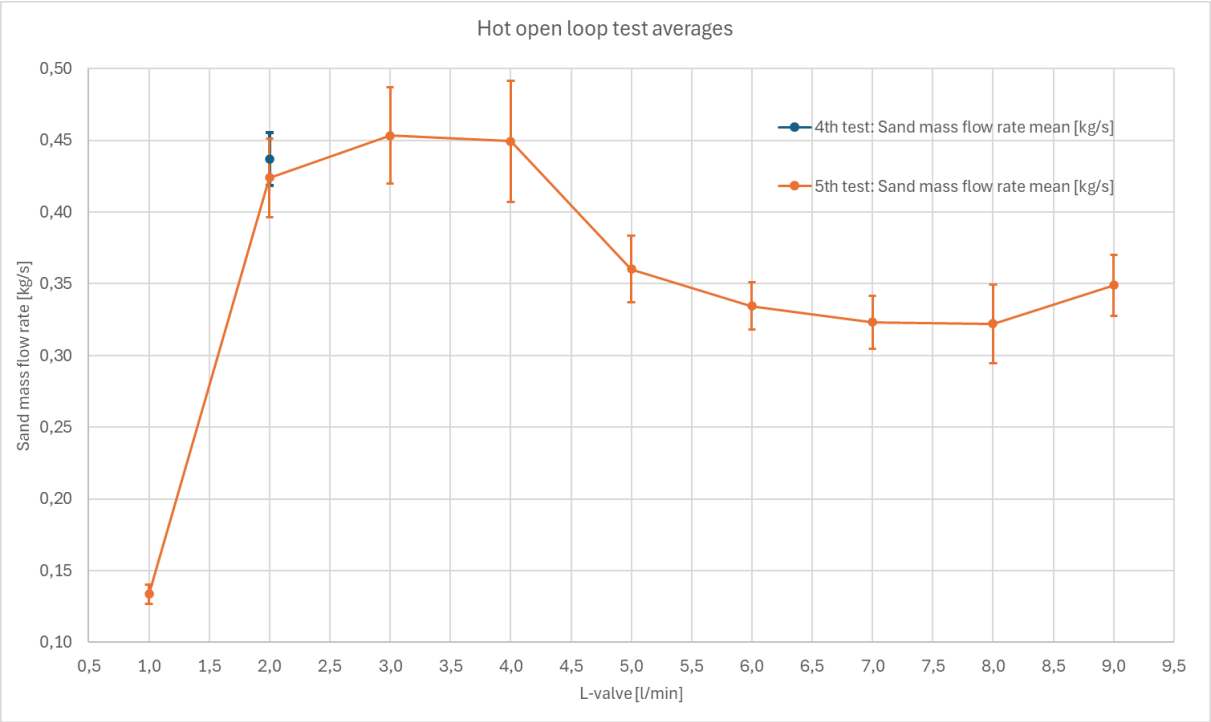

Figure 18. Hot open loop test averages (Korhonen, 2025m)

In the fourth test, slightly higher sand mass flow rate was achieved when the L-valve was set to 2 l/min, even though the reactor fluidization was lower than in test five. Therefore, in the fluidization region above 4,8 m/s, the sand mass flow rate is unaffected by the fluidization and is linearly dependent on the L-valve aeration if the L-valve aeration is in the range of 1 – 2 l/min.

In test five, the maximum mass flow rate was achieved when the L-valve was in the range between 2 – 4 l/min, while SEM began to increase after 2 l/min meaning that the reactor was unstable. Therefore, operating values for the L-valve are between 1 – 2 l/min.

It is noticeable that the SEM diminished by 33 % in test four compared to test five. In the fourth test, five repetitions were completed with L-valve aeration of 2 l/min, achieving an SEM value of 0,018. In the fifth test, one repetition was completed with L-valve aeration of 2 l/min, achieving an SEM value of 0,027. However, during the implementation of test setup, the accuracy of a single test is sufficient to continue with following tests. Precise results become valuable when perfecting the setup.

5.8 Sixth and seventh test

The objective of the following cold and hot closed loop test was to do a series of test runs by increasing L-valve flow rate by 0,5 l/min starting from 0 l/min and ending to 9,5 l/min. The test was conducted to determine the maximum capacity of the reactor and to gain insight from the reactor behaviour, and to inspect the differences of cold and hot sand. The test setup is shown in (Figure 19).

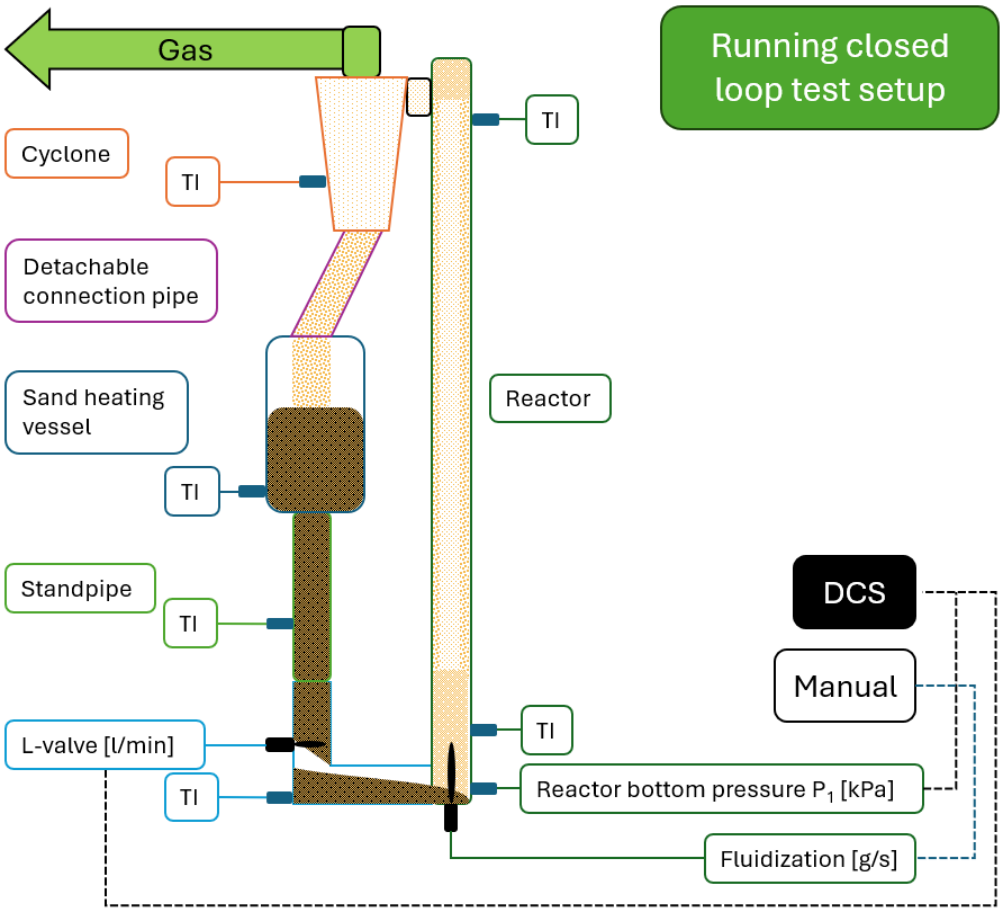

Figure 19. Modified test setup (Korhonen, 2025n)

For this test, setup had to modified due to faulty readings from the pressure difference gauge. Pressure line P_2 was removed, and the pressure was measured from the bottom of the reactor. A total of 20 repetitions were performed, as shown in (Figure 20 and Figure 21).

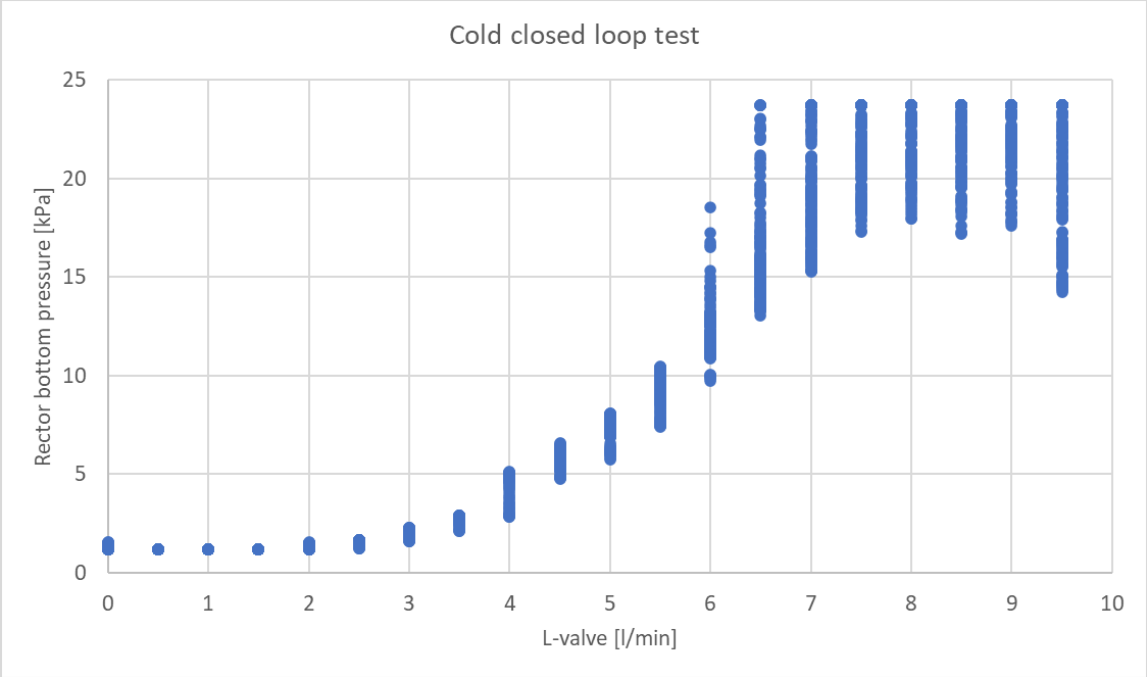

Figure 20. Cold closed loop test (Korhonen, 2025o)

Based on the Figure 20, the L-valve operating area in cold reactor compared to the reactor bottom pressure is from 0 l/min to 5,5 l/min. When the L-valve reached 6 l/min, the reactor pressure began to fluctuate increasingly in increments of 0,5 l/min. This is an indication of choking or slugging in the reactor. As a note the measurable maximum pressure was 23,7 kPa. Therefore, the actual fluctuation might be more than the figure indicates.

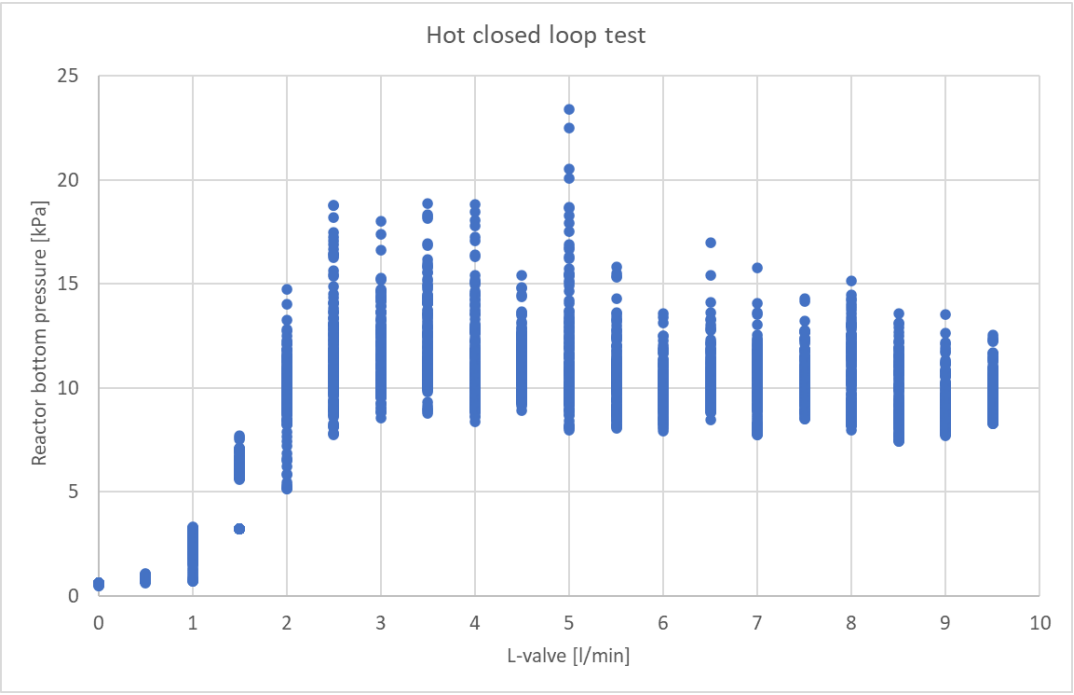

Figure 21. Hot closed loop test (Korhonen, 2025p)

L-valve operating area, in the hot reactor compared to the bottom reactor pressure, is from 0 l/min to 1,5 l/min based on the (Figure 21). Pressure starts fluctuating increasingly at 2 l/min which is an indication of choking or slugging.

When comparing sand behavior of cold and hot sand, it noticeable that the hot sand flows to the reactor at lower L-valve aeration values than cold sand. This is because an increase in temperature causes the gases to expand, which increases their volumetric flow rate and gas viscosity.

6 TEST RESULTS ANALYSIS

Test results are presented in (Table 4). Seven test campaigns were conducted using different parameters to find the bed material mass flow rate and to answer research questions. Even though, tests one and two did not produce any targeted results, they are presented for clarity.

Table 4. Test results

Test	Method	Parameters	Objective	Result	SEM [%]
1	Manual stop	Temp: ambient Reactor fluidization: 15 g/s L-valve: 4 l/min	Mass flow rate	Not accurate enough	
2	Automatic stop	Temp: ambient Reactor fluidization: 15 g/s L-valve: 4 l/min	Mass flow rate	Not accurate enough	
3	Open	Temp: 13 – 32 ºC Reactor fluidization: 15 g/s L-valve: 4 – 5 – 6 – 7 – 8,3 – 9,7 l/min	Mass flow rate as a function of L-valve aeration	4 – 9,7 l/min, 0,19 – **0,38 kg/s**	± 1,74 – 5,97
4	Open	Temp: 491 – 534 ºC Reactor fluidization: 5,5 g/s L-valve: 2 l/min	Accurate mass flow rate	**0,44 kg/s**	± 4,22
5	Open	Temp: 485 – 550 ºC Reactor fluidization: 12 g/s L-valve: 1 – 9 in steps of 1	Mass flow rate as a function of L-valve aeration	1 – 9 l/min, 0,13 – **0,45 kg/s**	± 4,83 – 9,44
6	Closed	Temp: 6 – 9 ºC Reactor fluidization: 15 g/s L-valve: 0 – 9,5 in steps of 0,5	Reactor max capacity	**5,5 l/min**, 9,3 kPa	
7	Closed	Temp: 498 – 565 ºC Reactor fluidization: 5,5 g/s L-valve: 0 – 9,5 in steps of 0,5	Reactor max capacity	**1,5 l/min**, 5,5 kPa	

Note: In tests 1 and 2, temperature data was not available.

The maximum cold sand mass flow rate of 0,38 kg/s (SEM of ± 5,97 %) was reached when L-valve aeration was 7 l/min and the maximum hot sand mass flow rate of 0,45 kg/s (SEM 9,44 %) was reached when L-valve aeration was 4 l/min. More accurate result for hot sand mass flow rate was 0,44 kg/s (SEM 4,22 %). When using hot sand, mass flow rate increased by 0,07 kg/s and the L-valve aeration dropped 3 l/min.

In the cold tests, the reactor maximum capacity of 5,5 l/min was reached at a reactor bottom pressure of 9,3 kPa, and in the hot tests, the reactor maximum capacity of 1,5 l/min was reached at reactor bottom pressure of 5,5 kPa.

6.1 Measurement errors and corrective actions

Several uncertainties were identified during testing that affected measurement accuracy. The first problems occurred in test one and two. The pressure difference gauge was giving faulty readings. It was assumed that the pressure line P_2 was clogged. As an immediate solution the, P_2 pressure line was removed, and the pressure was measured only from the bottom of the reactor. To permanently resolve the problem the P_2 measuring point could be relocated.

The temperature of the sand varied during the hot and cold test runs. The highest temperature difference of 67 ºC was measured in test seven. An increase in temperature causes gas expansion and an error of ± 4,6 % in the reactor fluidization velocity. However, as learned from tests 4 – 5, an increase after 4,8 m/s in reactor gas fluidization velocity does not affect the sand mass flow rate. Reasons for the temperature difference included the low thermal conductivity of sand, the positioning of thermoelements, and the insulation around the system (Tetteh, et al., 2024). Before starting the test, the sand and process lines were heated by thermoelements. At the start of the process, it was observed that rector temperature decreased, indicating that the sand was not completely heated from the middle or that the process lines were cold. It was also noted that the thermoelements left cold spots, especially in the corners. Additionally, the setup was regularly opened, which meant removal of insulation causing gaps between the insulation elements. As a solution, the sand should pre-circulate before the test long enough to ensure that the temperature does not vary.

During hot sand tests four and five, standpipe and L-valve were clogged multiple times. Therefore, multiple tests needed to be redone to get accurate results. It was assumed that ash-like compounds, such as alkali metal salts, could melt at hot temperature and form a sticky substance. The standpipe could have multiple aeration points to keep the solids in a fluidized state. Insufficient aeration in the standpipe can cause the solids to settle near the bottom, leading to less pressure buildup in standpipe and a decrease in solids flow through the L-valve (Knowlton, 1997).

Tests six and five revealed that the reactor presented choking or slugging at higher L-valve aeration values. This could be seen as spiking pressure measurements in (Figure 18 and Figure 19). The reactor disturbance was also visible and caused mechanical vibration. The reactor disturbances could be reduced by changing the length-diameter ratio of the reactor (Xiao, et al., 2024).

In conclusion, testing revealed multiple issues that affected the accuracy of test results and process stability. Problems included faulty pressure readings, temperature variations, and flow disturbances. These factors required immediate corrective action to the setup and consideration of their impact on measurement errors. For long-term improvements, efforts should focus on temperature control, aeration design, and adjustments to the reactor geometry to reduce operational disturbances. However, since the setup is modified according to the following test, long-term solutions are hard to make.

6.2 Ethics and reliability

In this thesis, ethics and reliability were considered according to the basic principles of research integrity as outlined in the European Code of Conduct. The core principals were reliability, honesty, respect, and accountability. The research practice consisted of methods that ensured research integrity was maintained throughout the life span of the research (TENK, 2023).

7 DISCUSSION

The thesis work was structured around four phases: idea formulation, practical implementation, data analysis, and writing of the report. My own work during these phases was consistent and followed the thesis work plan. In my thesis, I was able to answer the research question that had been set. Therefore, the research of plastic pyrolysis can continue with a new set of questions.

Throughout the separate phases mentioned earlier, I was able to improve my skills in project planning, independent research, and scientific writing. Also, during the practical implementation I gained direct experience in conducting experiments, collecting, and analyzing data, and how to solve unexpected challenges. These experiences have strengthened my readiness for the future.

One of the successes of the thesis was the scope. The thesis was strictly limited to the purpose and to the research questions. This made writing the thesis relatively easy as the goal was clear. For the next research paper, I would consider writing the research section first, followed by the theoretical background. This way it is easier to write theory to support findings. Also, I would use more time to think about the research questions and how the timeline would go during the thesis work.

In the future, constraints related to sand mass flow rate should be investigated further. Based on the results from tests four and five, the limiting factors of mass flow rate does not appear to be reactor fluidization, but another unknown variable. For future research, the focus will be on identifying optimal pyrolysis parameters for different feedstocks to maximize the yield. Some of the key research questions include reactor temperature and residence time in the reactor.

REFERENCES

Microsoft. 2025. Copilot. GPT-4. Accessed for language check, November 2025. https://copilot.microsoft.com

Al-Salem, S., Lettieri, P. & Baeyens, J., 2010. The valorization of plastic solid waste (PSW) by primary to quaternary routes: From re-use to energy and chemicals. *Progress in Energy and Combustion Science,* 36(1), pp. 103-129.

Chen, Y.-H., Hsieh, W., Chang, H. & Ho, C.-D., 2022. Design and economic analysis of industrial-scale methanol-to-olefins plants. *Journal of the Taiwan Institute of Chemical Engineers,* Volume 130.

Dai, L. et al., 2022. Pyrolysis technology for plastic waste recycling: A state-of-the-art review. *Progress in Energy and Combustion Science,* Volume 93.

Dayana Anuar Sharuddin, S., Abnisa, F., Daud, W. M. A. W. & Aroua, M. K., 2016. Energy Conversion and Management. *A review on pyrolysis of plastic wastes,* Volume 115, pp. 308-326.

Dogu, O. et al., 2021. The chemistry of chemical recycling of solid plastic waste via pyrolysis and gasification: State-of-the-art, challenges, and future directions. *Progress in Energy and Combustion Science,* Volume 84.

Eskanlou, A. & Arnold, B. J., 2025. An evaluation of quartz as a component of respirable coal dust. *Journal of Hazardous Materials,* Volume 490.

Fescon Technology, 2025. *Seulontatodistus,* s.l.: s.n.

Geyer, R., Jambeck, J. R. & Law, K. L., 2017. Production, use, and fate of all plastics ever made. *Science advances,* 3(7), p. 5.

Grace, J. R. & Bi, H., 1997. Introduction to circulatin fluidized beds. In: J. Grace, A. Avidan & T. Knowlton, eds. *Circulatin fluidized beds.* London: Blackie Academic and Professional an imprint of Chapman, pp. 1-20.

Hassani, H. & Ghodsi, M., 2010. A note on standard deviation and standard error. *Teaching Mathematics and its Applications,* pp. 108-112.

Horio, M., 2010. Particuology. *Fluidization science, its development and future,* 8(6), pp. 514-524.

Kalali, E. N. et al., 2023. A critical review of the current progress of plastic waste recycling technology in structural materials. *Current Opinion in Green and Sustainable Chemistry,* Volume 40.

Khatun, R. et al., 2021. Bibliometric analysis of research trends on the thermochemical conversion of plastics during 1990–2020. *Journal of Cleaner Production,* Volume 317.

Knowlton, T. M., 1997. Standpipes and return systems. In: J. Grace, A. A. Avidan & T. Knwolton, eds. *Circulating fluidized beds.* London: Blackie Academic and Professional, pp. 214-259.

Korhonen, J., 2025a. *Typical CFB configuration.* Tampere: s.n.

Korhonen, J., 2025b. *Running closed loop test setup.* Tampere: s.n.

Korhonen, J., 2025c, CC-BY. *Measuring cup.* Tampere: s.n.

Korhonen, J., 2025d, CC-BY. *Sand bucket on a scale.* Tampere: s.n.

Korhonen, J., 2025e. *Starting point of cold closed loop stop test.* Tampere: s.n.

Korhonen, J., 2025f. *Running cold closed loop test.* Tampere: s.n.

Korhonen, J., 2025g. *Cold stop test No. 9.* Tampere: s.n.

Korhonen, J., 2025h. *Faulty pressure line.* Tampere: s.n.

Korhonen, J., 2025i. *Starting point of cold open loop test.* Tampere: s.n.

Korhonen, J., 2025j. *Running open loop cold test.* Tampere: s.n.

Korhonen, J., 2025k. *Scale calibration data analysis.* Tampere: s.n.

Korhonen, J., 2025l. *Cold open loop test averages.* Tampere: s.n.

Korhonen, J., 2025m. *Hot open loop test averages.* Tampere: s.n.

Korhonen, J., 2025n. *Modified test setup.* Tampere: s.n.

Korhonen, J., 2025o. *Cold closed loop test.* Tampere: s.n.

Korhonen, J., 2025p. *Hot closed loop test.* Tampere: s.n.

Korhonen, J., 2025q. *Pressure difference faulty readings.* Tampere: s.n.

Kunii, D. & Levenspiel, O., 1991. Industrial Applications of Fluidized Beds. In: *Fluidization Engineering.* Boston: Butterworh-Heinemann, pp. 1-17.

Liu, Q. et al., 2024. The role of plastic chemical recycling processes in a circular economy context. *Chemical Engineering Journal,* Volume 498.

Mallick, R., Vairakannu, P. & Shiju, N. R., 2025. Plastics waste to olefins in a circular economy: Techno-economic and life cycle comparison of hydrothermal liquefaction and pyrolysis. *Journal of Cleaner Production,* Volume 530.

Miao, Y., Von Jouanne, A. & Yokochi, A., 2021. Current Technologies in Depolymerization Process and the Road Ahead. *Polymers 2021,* Volume 13.

Muschelknautz, E. & Greif, V., 1997. Cyclones and other-gas solids separators. In: J. Grace, A. Avidan & T. Knowlton, eds. *Circulating fluidized beds.* London: Blackie Academic and professional, pp. 181-213.

Peng, Y. et al., 2022. A review on catalytic pyrolysis of plastic wastes to high-value products. *Energy Conversion and Management,* Volume 254.

Peterson, D., 2023. *Siemens TIA Portal and S7-1200 Tutorial 2: Analog Inputs.* [Online]
Available at: https://control.com/technical-articles/siemens-tia-portal-and-s7-1200-tutorial-2-analog-inputs/
[Accessed 31 10 2025].

Pilapitiya, P. N. T. & Ratnayake, A. S., 2024. The world of plastic waste: A review. *Cleaner Materials,* Volume 11.

Plastics Europe, 2025. *Plastics the Fast Facts 2025,* s.l.: s.n.

Ragaert, K., Delva, L. & van, G. K., 2017. Mechanical and Chemical Recycling of Solid Plastic Waste. *Waste Management,* Volume 69, pp. 24-58.

Saikrishnan, S., Jubinville, D., Tzoganakis, C. & Mekonnen, T. H., 2020. Thermo-mechanical degradation of polypropylene (PP) and low-density polyethylene (LDPE) blends exposed to simulated recycling. *Polymer Degradation and Stability,* Volume 182.

SFS, 2012. *Tests for general properties of aggregates. Part 1: Methods for sampling.* [Online]
Available at: https://sales.sfs.fi/fi/index/tuotteet/SFS/CEN/ID2/9/177763.html.stx
[Accessed 18 11 2025].

SFS, 2012. *Tests for general properties of aggregates. Part 1: Methods for sampling.* [Online]
Available at: https://sales.sfs.fi/fi/index/tuotteet/SFS/CEN/ID2/9/177763.html.stx
[Accessed 18 11 2025].

SFS, 2012. *Tests for geometrical properties of aggregates. Part 1: Determination of particle size distribution. Sieving method.* [Online]
Available at: https://sales.sfs.fi/fi/index/tuotteet/SFS/CEN/ID2/9/193449.html.stx
[Accessed 18 11 2025].

SFS, 2015. *Protective clothing. Clothing to protect against heat and flame. Minimum performance requirements (ISO 11612:2015).* [Online]
Available at: https://sales.sfs.fi/fi/index/tuotteet/SFS/CENISO/ID2/1/397610.html.stx
[Accessed 18 11 2025].

SFS, 2020. *Hearing protectors. General requirements. Part 1: Earmuffs.* [Online]
Available at: https://sales.sfs.fi/fi/index/tuotteet/SFS/CEN/ID2/3/946982.html.stx
[Accessed 18 11 2025].

SFS, 2022. *Eye and face protection for occupational use. Part 3: Additional requirements for mesh protectors (ISO 16321-3:2021).* [Online]
Available at: https://sales.sfs.fi/fi/index/tuotteet/SFS/CENISO/ID2/1/1117687.html.stx
[Accessed 18 11 2025].

SFS, 2022. *Personal protective equipment. Safety footwear (ISO 20345:2021).* [Online]
Available at: https://sales.sfs.fi/fi/index/tuotteet/SFS/CENISO/ID2/2/1107472.html.stx
[Accessed 18 11 2025].

SFS, 2025. *Industrial protective helmets.* [Online]
Available at: https://sales.sfs.fi/en/index/tuotteet/SFS/CEN/ID2/3/1352506.html.stx
[Accessed 18 11 2025].

Sing, R. K., Ruj & Biswajit, 2016. Time and temperature depended fuel gas generation from pyrolysis of real world municipal plastic waste. *Fuel,* Volume 174, pp. 164-171.

Solis, M. & Silveira, S., 2020. Technologies for chemical recycling of household plastics – A technical review and TRL assessment. *Waste Management,* Volume 105, pp. 128-138.

TENK, F. N. B. o. R. I., 2023. *The Finnish Code of Conduct for Research Integrity and Procedures for Handling Alleged Violations of Research Integrity in Finland.* [Online]
Available at: https://tenk.fi/sites/default/files/2023-11/RI_Guidelines_2023.pdf
[Accessed 17 9 2025].

Tetteh, S., Juul, G., Järvinen, M. & Santasalo-Aarnio, A., 2024. Improved effective thermal conductivity of sand bed in thermal energy storage systems. *Journal of Energy Storage,* Volume 86.

Timsina, R., Thapa, R., Moldestad, B. M. E. & Eikeland, M., 2022. Methanol Synthesis from Syngas: a Process Simulation. *Scandinavian Simulation Society,* pp. 444-449.

Valmet, 2025. *Henkilösuojaimet ja työvaatteet.* [Online]
[Accessed 18 11 2025].

Xiao, H. et al., 2024. Investigating choking phenomena in CFB risers under different operating parameters. *Powder Technology,* Volume 440.

Zhang, K. et al., 2021. Understanding plastic degradation and microplastic formation in the environment: A review. *Environmental Pollution,* Volume 274.

APPENDIX 1: GLOBAL PLASTIC PRODUCTION BY SOURCE

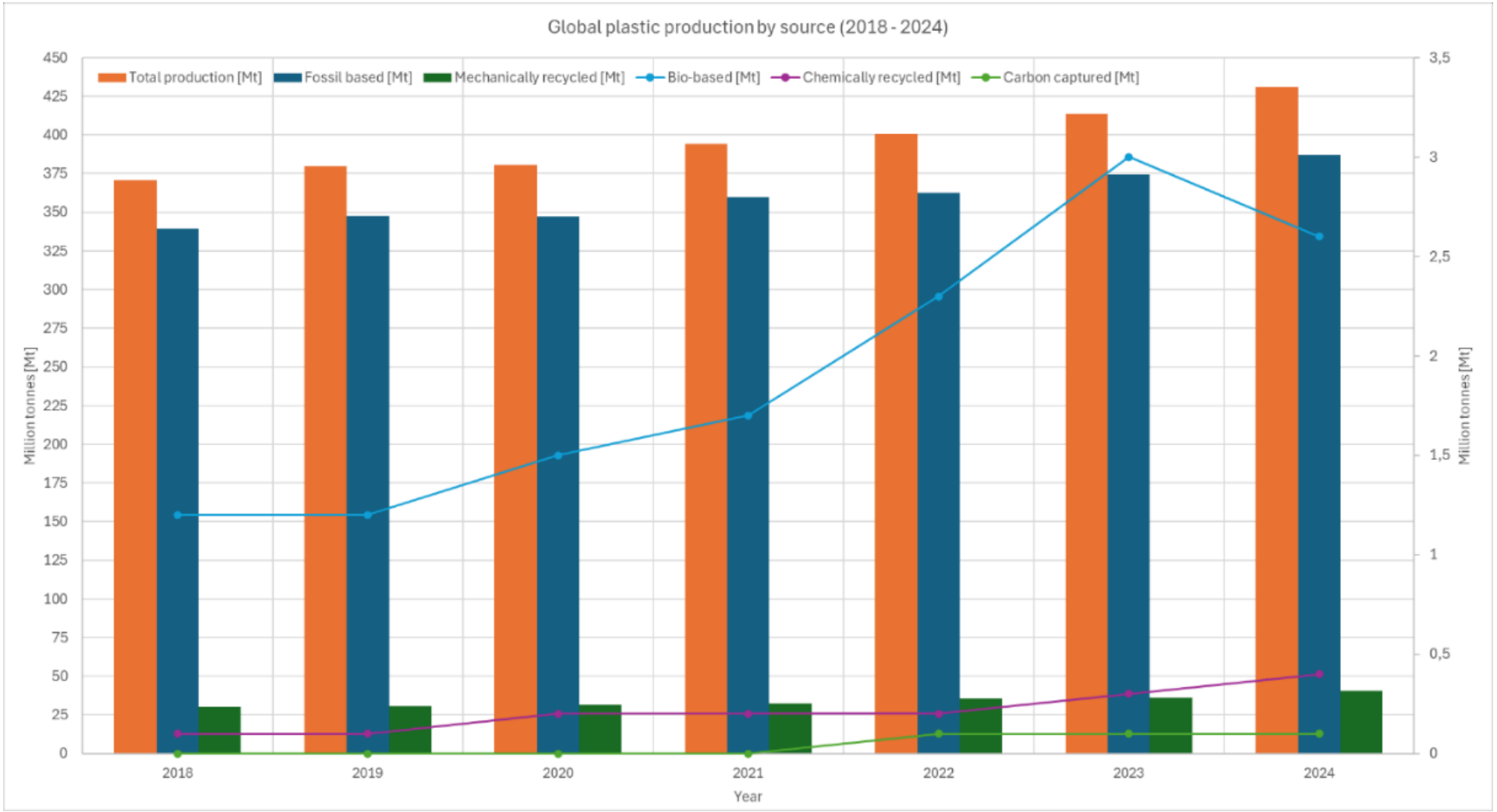

Figure 22. Global plastic production by source (2018 – 2024), adapted from (Plastics Europe, 2025). The column values are shown on the left Y-axis, and the line values are shown on the right Y-axis

APPENDIX 2: ANALYSED DATA FROM THE TEST

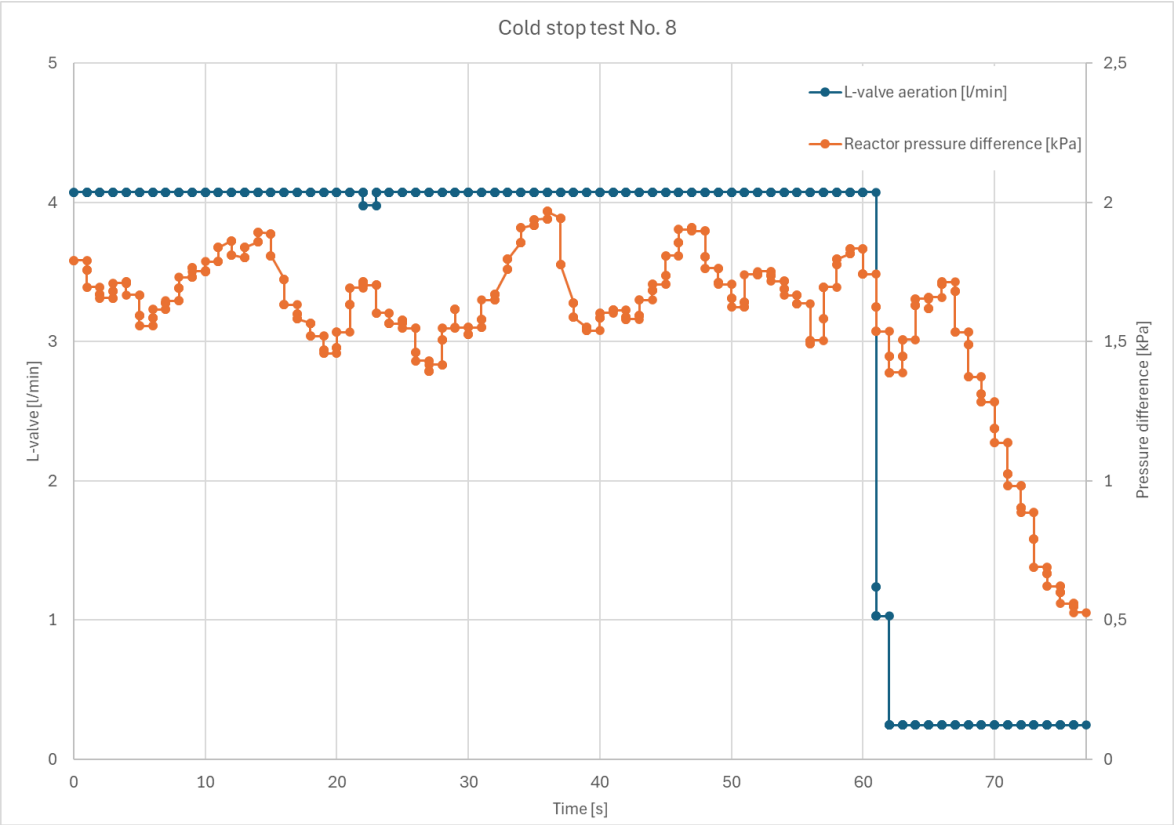

Figure 23. Pressure difference faulty readings (Korhonen, 2025q)